

Control of the transient behaviour of polymer electrolyte membrane fuel cell systems

M Grujic^{1*}, K M Chittajallu¹ and J T Pukrushpan²

¹Department of Mechanical Engineering, Clemson University, Clemson, South Carolina, USA

²Department of Mechanical Engineering, University of Michigan, Ann Arbor, Michigan, USA

Abstract: The transient behaviour of a polymer electrolyte membrane fuel cell (PEMFC) system following abrupt changes in the stack current is analysed using a non-linear dynamic, control-oriented computer model. Such changes in the stack current are associated with the abrupt changes in power demanded by a vehicle powered by the fuel cell system. The PEMFC system analysed consists of air and fuel supply subsystems, a perfect air/fuel humidifier, and a fuel cell stack, and is assumed to operate under a constant fuel cell temperature. The model is next used to develop a feedback control scheme to regulate the transient behaviour of the PEMFC system with respect to maintaining the necessary level of the oxygen partial pressure in the cathode following abrupt changes in the stack current demanded by the user. Maintaining the level of oxygen in the cathode is critical to prevent short circuit and membrane damage. The results obtained indicate that the oxygen level in the cathode can be successfully maintained using a feedback control of the air-compressor-motor voltage. However, the net power provided by the fuel cell system is compromised during the transients following abrupt changes in the stack current, suggesting a need for power management via a secondary power source, such as an electric battery.

Keywords: polymer electrolyte membrane fuel cells, feedback control

NOTATION

I	current (A)
K	gain factor
m	mass (kg)
p	pressure (Pa)
t	time (s)
T	temperature (K)
v	voltage (V)
V	volume (m ³)
W	flow rate (kg/s)
ε	linearized system eigenvalue
λ	excess ratio
τ	torque (Nm)
ω	rotational speed (rad/s)

Subscripts

An	anode-related quantity
atm	quantity at 1 atm pressure
c	canonical form of the quantity
Ca	cathode-related quantity
CM	compressor-motor-related quantity
Cp	compressor-related quantity
d	desired value of a quantity
gen	quantity generated through electrochemical reaction
H ₂	hydrogen-related quantity
in	inlet quantity
I	integral-control quantity
m	membrane-related quantity
net	net quantity
N ₂	nitrogen-related quantity
out	outlet quantity
Obs	observer-related quantity
O ₂	oxygen-related quantity
P	proportional-control quantity
react	quantity consumed in electrochemical reaction

The MS was received on 2 August 2003 and was accepted after revision for publication on 9 June 2004.

* Corresponding author: Department of Mechanical Engineering, Clemson University, 241 Engineering Innovation Building, Clemson, SC 29634-0921, USA. email: mica.grujic@ces.clemson.edu

RM	quantity associated with the return manifold for cathode
st	fuel cell stack-related quantity
SM	quantity associated with the supply manifold for cathode
v	water-vapour-related quantity
w	liquid-water-related quantity

Superscripts

max	maximum value
o	nominal value
opt	optimal value

The remaining quantities are defined in Tables 1 and 2.

Table 1 General parameters used for modeling the PEMFC

Parameter	Symbol	SI units	Value
Atmospheric pressure	p_{atm}	Pa	1.013×10^5
Atmospheric temperature	T_{atm}	K	298.15
Air-specific heat ratio	γ	–	1.4
Air-specific heat	C_p	J/kg/K	1004
Air density	ρ_a	kg/m ³	1.23
Universal gas constant	R	J/mol/K	8.314
Air gas constant	R_a	J/kg/K	286.9
Oxygen gas constant	R_{O_2}	J/kg/K	259.8
Nitrogen gas constant	R_{N_2}	J/kg/K	296.8
Vapour gas constant	R_v	J/kg/K	461.5
Hydrogen gas constant	R_{H_2}	J/kg/K	4124.3
Molar mass of air	M_a	kg/mol	28.97×10^{-3}
Molar mass of oxygen	M_{O_2}	kg/mol	32.0×10^{-3}
Molar mass of nitrogen	M_{N_2}	kg/mol	28.0×10^{-3}
Molar mass of vapour	M_v	kg/mol	18.02×10^{-3}
Molar mass of hydrogen	M_{H_2}	kg/mol	2.0×10^{-3}
Faraday's constant	F	A·s/mol	96 487
Temperature of the FC	T_{fc}	K	353

1 INTRODUCTION

Vehicles powered by fuel cells (FCs) are still in the developmental stage. From a technical point of view they should be considered as electric vehicles since electricity generated by the fuel cell is used to drive an electric motor. However, the vehicle does not have to recharge as an electric vehicle does; instead, the fuel cell is filled up with a liquid (or gaseous) fuel, in the same way that the fuel tank of an internal combustion (IC) engine vehicle (such as gasoline or diesel) is filled up.

One of the most promising FCs is the so-called polymer electrolyte membrane or proton exchange membrane (PEM) FC. A membrane is a medium that separates the anode and the cathode in a FC. Electrons liberated during fuel oxidation in the anode travel through an external circuit (containing an electric motor) until they reach the cathode. Inside the cathode, the electrons combine with the protons (also generated in the anode, but diffuse through the membrane to the cathode) to reduce oxygen and form water. While a single PEMFC typically produces a voltage of ~ 0.7 V at a nominal current density of 1 A/cm², the voltage can be increased by stacking FCs in series, in which case the stack voltage is simply equal to the product of a single FC operation voltage and the number of cells in the stack.

Owing to their high energy efficiency, low temperature (~ 333 – 353 K) operation, pollution-free character, and relatively simple design, PEMFCs are currently being considered as an alternative source of power in electric vehicles. However, in order to be able to successfully compete with IC engines, PEMFCs must operate and function at least as well as them. Specifically, the transient behaviour of PEMFCs, following abrupt changes

Table 2 Input parameters used for modeling the PEMFC

Parameter	Symbol	SI units	Value
Motor constant	k_t	Nm/A	0.0153
Motor constant	R_{CM}	ohm	0.82
Motor constant	k_v	V/(rad/s)	0.0153
Compressor efficiency	η_{Cp}	–	0.80
Compressor motor mechanical efficiency	η_{CM}	–	0.98
Number of cells in FC stack	n	–	381
FC active area	A_{fc}	m ²	280×10^{-4}
Supply manifold volume	V_{SM}	m ³	0.02
Single stack cathode volume	V_{Ca}	m ³	0.01
Single stack anode volume	V_{An}	m ³	0.005
Return manifold volume	V_{RM}	m ³	0.005
Supply manifold outlet orifice constant	$k_{SM, out}$	kg/s/Pa	0.3629×10^{-5}
Cathode outlet orifice constant	$k_{Ca, out}$	kg/s/Pa	0.2177×10^{-5}
Membrane dry density	$\rho_{m, dry}$	kg/m ³	2×10^3
Membrane dry equivalent weight	$M_{m, dry}$	kg/mol	1.1
Membrane thickness	t_m	m	1.275×10^{-4}
Compressor diameter	d_{Cp}	m	0.2286
Compressor and motor inertia	J_{Cp}	kg·m ²	5×10^{-5}
Return manifold throttle discharge coefficient	C_D	–	0.0124
Return manifold throttle area	A_T	m ²	0.002
Average ambient air relative humidity	ϕ_{atm}	–	0.5
Oxygen mole fraction at cathode inlet	$x_{O_2, in}$	–	0.21
Hydrogen mole fraction at anode inlet	$x_{H_2, in}$	–	1.0

in the power demanded by the vehicle, is particularly critical since it entails control of the air and fuel flows, pressure regulation, and heat and water management to maintain optimal temperature, membrane hydration, and partial pressure of the reactants. Such regulations are necessary in order to avoid degradation in the FC stack voltage and in the energy efficiency, as well as to help extend the FC's life [1].

Over the last decade, a number of FC models have been developed. Most of these models, including the ones developed in our research group [2–4], are steady state, single-cell models, which include spatial variation of the FC parameters and are based on electrochemical, thermodynamic, and fluid mechanical principles. Consequently, these models are not suitable for analysis and control of the transient behaviour of FCs.

Among the dynamic FC models proposed so far, most of them address the issues specific to the control of particular FC subsystems [e.g. 5–6]. Recently, Pukrushpan *et al.* [7–8] proposed a FC system dynamic model suitable for control of FC transient behaviour. The model deals with the FC stack system and includes the flow and inertia characteristics of the air compressor, cathode, and anode manifold filling dynamics. In our recent work [9], the model of Pukrushpan *et al.* was extended to include the effect of optimization of the oxygen excess ratio in the cathode, which yields a maximal net power at a given level of FC stack current. In the present work, feedback control of the transient behaviour of PEMFCs following abrupt changes in the power demanded by the vehicle is considered.

The organization of the paper is as following: the model of Pukrushpan *et al.* is briefly overviewed in sections 2.1–2.3; the problem of control of the transient behaviour of a PEMFC system is formulated in section 2.4; the computational procedure used is discussed in section 3; the main results obtained in the present work are presented and discussed in section 4; and the main conclusions resulting from the present work are summarized in section 5.

2 THE MODEL

Control-oriented models of FC systems have a number of salient features, such as:

- they include dynamic (transient) effects, while the effects of spatial variation of the model parameters are neglected;
- since the dynamics of electrochemical reactions and of the electrodes' electrical response are associated with very fast transients, their effects on the overall FC system transient performance is minimal and is neglected;
- transient behaviour of the manifold filling, of the membrane hydration, of the air compressor, and of

- the heat management are significantly more sluggish and, hence, should be included in the model;
- interactions between the processes identified in (c) should also be taken into account;
- owing to its relatively slow transient response, the dynamics of the FC stack temperature may play an important role; however, the stack temperature is generally considered to be controlled separately from the rest of the FC system and its average value to be well regulated; and
- the humidity and temperature of the inlet reactant flows in the cathode and the anode are generally assumed to be controlled in a fast manner so that their transient behaviours are generally not considered.

In this section, a brief overview is given of the FC stack dynamic model proposed by Pukrushpan *et al.* [7–8]. A schematic of the PEMFC system analysed in the model is shown in Fig. 1.

2.1 The state space representation

The model proposed by Pukrushpan *et al.* [7–8] uses the following nine states:

- The mass of oxygen in the cathode, m_{O_2} (kg).
- The mass of nitrogen in the cathode, m_{N_2} (kg).
- The mass of water in the cathode, $m_{w, Ca}$ (kg).
- The mass of hydrogen in the anode, m_{H_2} (kg).
- The mass of water in the anode, $m_{w, An}$ (kg).
- The compressor speed, ω_{Cp} (rad/s).
- The supply manifold pressure, p_{SM} (Pa).
- The mass of air in the supply manifold, m_{SM} (kg).
- The return manifold pressure, p_{RM} (Pa).

2.2 The governing equations

The governing equations for the mass of air in the supply manifold, for the masses of oxygen, nitrogen, and water in the cathode, and for the masses of hydrogen and water in the anode, are respectively defined using the

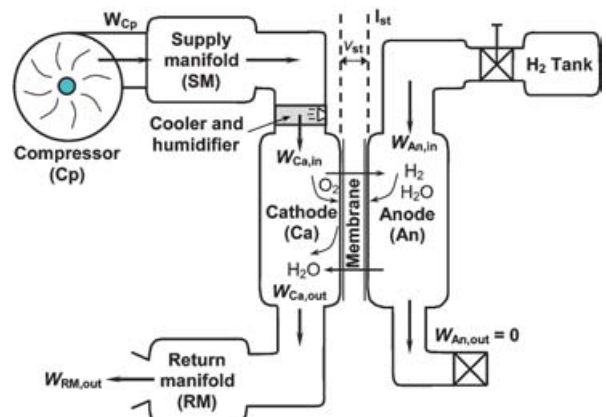


Fig. 1 Components and volumes in a PEMFC reactant supply system

principle of mass conservation as

$$\frac{dm_{SM}}{dt} = W_{Cp} - W_{Sm, out} \quad (1)$$

$$\frac{dm_{O_2}}{dt} = W_{O_2, in} - W_{O_2, out} - W_{O_2, react} \quad (2)$$

$$\frac{dm_{N_2}}{dt} = W_{N_2, in} - W_{N_2, out} \quad (3)$$

$$\frac{dm_{w, Ca}}{dt} = W_{v, Ca, in} - W_{v, Ca, out} + W_{v, Ca, gen} + W_{v, m} \quad (4)$$

$$\frac{dm_{H_2}}{dt} = W_{H_2, in} - W_{H_2, out} - W_{H_2, react} \quad (5)$$

$$\frac{dm_{w, An}}{dt} = W_{v, An, in} - W_{v, An, out} - W_{v, m} \quad (6)$$

The governing equation for the rotational speed of the compressor is defined by the power conservation principle as

$$J_{Cp} \frac{d\omega_{Cp}}{dt} = (\tau_{CM} - \tau_{Cp}) \quad (7)$$

The governing equations for the supply manifold pressure and the return manifold pressure are respectively defined, using the energy conservation principle and thermodynamic relationships, as

$$\frac{dp_{SM}}{dt} = \frac{\gamma R_a}{V_{SM}} (W_{Cp} T_{Cp} - W_{SM, out} T_{SM}) \quad (8)$$

$$\frac{dp_{RM}}{dt} = \frac{R_a T_{RM}}{V_{RM}} (W_{Ca, out} - W_{RM, out}) \quad (9)$$

2.3 Closure relations

To express the governing equations in terms of the states, the following closure relations are used.

The compressor airflow rate, W_{Cp} , is related to the supply manifold pressure, p_{SM} , and the compressor motor rotational speed, ω_{Cp} , via the appropriate static compressor map, as reviewed in Appendix A of reference [9]. The supply manifold outlet air rate, $W_{SM, out}$, is related to the p_{SM} and p_{Ca} via a linearized nozzle equation as

$$W_{SM, out} = k_{SM, out} (p_{SM} - p_{Ca}) \quad (10)$$

The inlet oxygen, nitrogen, and cathode-vapour mass flowrates, $W_{O_2, in}$, $W_{N_2, in}$, and $W_{v, Ca, in}$, are related to the cathode-inlet air mass flowrate, the inlet-air humidity, and the mass fraction of oxygen and nitrogen in dry air using the ideal gas relations.

The outlet oxygen, nitrogen, and cathode-vapour mass flowrates, $W_{O_2, out}$, $W_{N_2, out}$, and $W_{v, Ca, out}$, are related to the outlet air mass flowrate, the outlet air humidity, and the mass fraction of the oxygen and nitrogen in dry air at the cathode outlet, also using the ideal gas relations.

The reacted oxygen and hydrogen and generated water vapour (in the cathode) mass flowrates, $W_{O_2, react}$, $W_{H_2, react}$, and $W_{v, Ca, gen}$, are related to the FC stack current as

$$W_{O_2, react} = M_{O_2} \times \frac{nI_{st}}{4F} \quad (11)$$

$$W_{H_2, react} = M_{H_2} \times \frac{nI_{st}}{2F} \quad (12)$$

$$W_{v, Ca, gen} = M_v \times \frac{nI_{st}}{2F} \quad (13)$$

where 4 and 2 in the denominators of equations (11) to (13) denote the number of electrons involved in the oxidation and the reduction half-reactions respectively.

The water mass flowrate through the membrane, $W_{v, m}$, is defined using the membrane hydration model given in Appendix B of reference [9].

The outlet hydrogen and water mass in the anode are assumed to be zero, that is, hydrogen is assumed to react completely in the anode, while water generated by the oxidation half-reaction is assumed to be transported via electro-osmosis through the membrane towards the cathode.

The compressor motor torque, τ_{CM} , is related to the compressor motor voltage, v_{CM} , and the compressor motor rotational speed by the static motor equation as

$$\tau_{CM} = \eta_{CM} \frac{k_t}{R_{CM}} (v_{CM} - k_v \omega_{Cp}) \quad (14)$$

The steady state compressor torque, τ_{Cp} , is related to the supply manifold pressure, the compressor motor rotational speed and the compressor air flowrate via the thermodynamic relations as

$$\tau_{Cp} = \frac{C_p}{\omega_{Cp}} \frac{T_{atm}}{\eta_{Cp}} \left[\left(\frac{p_{SM}}{p_{atm}} \right)^{\gamma-1/\gamma} - 1 \right] W_{Cp} \quad (15)$$

The air temperature in the compressor, T_{Cp} , is defined using basic thermodynamic relations as

$$T_{Cp} = T_{atm} + \frac{T_{atm}}{\eta_{Cp}} \left[\left(\frac{p_{SM}}{p_{atm}} \right)^{\gamma-1/\gamma} - 1 \right] \quad (16)$$

The air temperature in the supply manifold, T_{SM} , is obtained from the m_{SM} , p_{SM} , and V_{SM} using the ideal gas law.

The cathode outlet air flowrate, $W_{Ca, out}$, is related to the cathode pressure and return manifold pressure via a linearized nozzle equation analogous to that in equation (10).

The return manifold outlet air flowrate, $W_{RM, out}$, is defined using a non-linearized nozzle relation, as discussed in Appendix C of reference [9], while the return manifold air temperature, T_{RM} , is considered as constant and equal to the temperature of the FC stack.

2.4 Control problem formulation

In a FC system, there are three main control systems that regulate:

- (a) the air/fuel supply;
- (b) the water supply; and
- (c) the heat management.

In the present model, a perfect air/fuel humidifier and a perfect air and stack cooler are postulated. In addition, a fast proportional feedback fuel-flow controller, which ensures a zero pressure difference across the membrane, is assumed. Therefore, the control problem discussed in the present work focuses on the regulation of the air (i.e. oxygen) supply to the cathode.

In our recent work [9], it was found that at each level of the stack current, there is an optimal value of the compressor motor voltage, v_{CM}^{opt} , which maximizes the stack net power, P_{net}^{max} . As shown in Fig. 2(a), a second-order polynomial in the form $v_{CM}^{opt} = -1.36 \times 10^{-3} I_{st}^2 + 1.17 I_{st} + 14.3$ was found to quite successfully represent the variation of the optimal v_{CM}^{opt} with I_{st} . When the current demand from the vehicle suddenly increases, the oxygen consumption in the cathode also increases and, hence, the oxygen partial pressure drops. The accompanying drop in the FC voltage may lead to a short circuit

and/or membrane damage, the phenomenon known as oxygen starvation. To prevent this from happening, the air supply must be promptly increased to replenish the cathode with oxygen. Also, the fuel supply to the anode must be quickly adjusted to ensure a minimal pressure difference across the FC membrane. A similar control of the FC system is required during a sudden drop in the stack current. Since not all state variables of the system can be measured directly, three variables: the compressor air flowrate, W_{Cp} , the supply manifold pressure, p_{SM} , and the FC stack voltage, v_{st} , are measured and used in the construction of a feedback control model.

Thus, the FC system control problem can be defined as

$$\begin{aligned} \dot{x} &= f(x, u, w) && \text{state equations} \\ x &= [m_{O_2} \ m_{H_2} \ m_{N_2} \ \omega_{Cp} \ p_{SM} \ m_{SM} \ m_{w, An} \ m_{w, Ca} \ p_{RM}]^T && \text{states} \\ u &= v_{CM} && \text{controlled variable} \\ w &= I_{st} && \text{disturbance} \\ z &= [z_1 = P_{net} - P_{net}^{max}, \ z_2 = \lambda_{O_2} - \lambda_{O_2}^{opt}]^T = h_z(x, u, w) && \text{performance variables} \\ y &= [W_{Cp}, p_{SM}, v_{st}]^T && \text{measurements} \end{aligned} \tag{17}$$

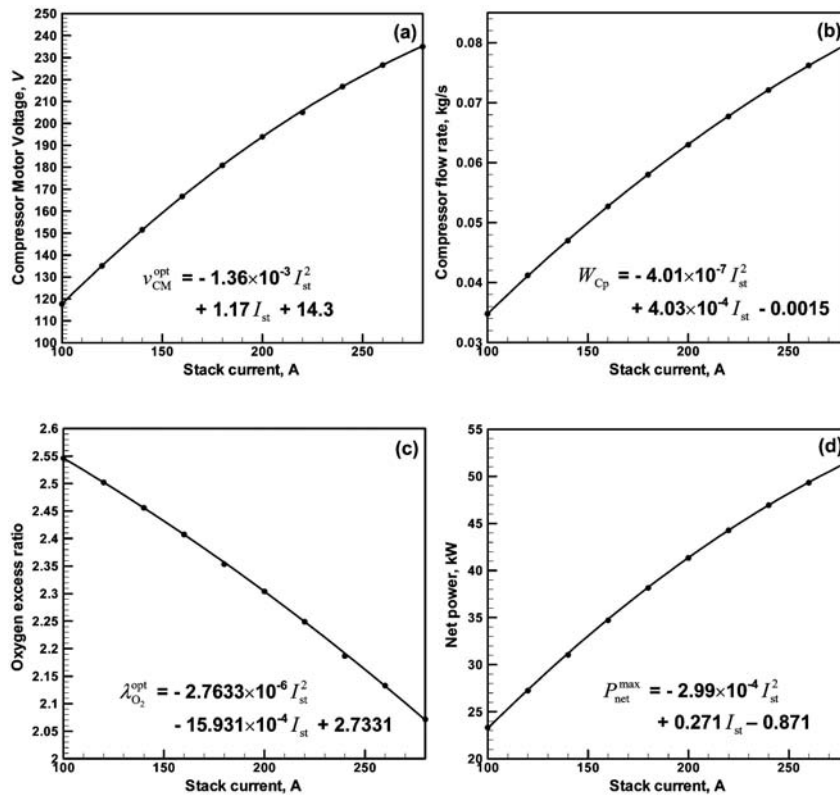


Fig. 2 (a) Optimal compressor-motor voltage; (b) optimal compressor flowrate; (c) optimal oxygen excess ratio; and (d) maximal net power as a function of stack current in a PEMFC under standard operating conditions

It should be noted that the two control objectives, $z_1 = z_2 = 0$, are achievable at steady state, but their transients are considerably different and, hence, cannot be controlled simultaneously using a single-control variable, v_{CM} . Owing to the above-mentioned undesirable consequences of oxygen starvation, only the control of the transient behaviour of λ_{O_2} will be considered in this work. The transient behaviour of the net power is monitored, but its control is not considered and will be assumed to be achieved through power management via a secondary power source (an electric battery). Furthermore, as mentioned above, the goal of the hydrogen flow control is to minimize the pressure difference across the membrane. Hydrogen is supplied to the anode from a high-pressure tank and its flowrate is controlled by a valve. Since the valve has a fast response, the hydrogen flowrate can be directly regulated using a proportional feedback controller based on the anode/cathode pressure difference. In practice, however, the cathode and anode pressures cannot be directly measured. To overcome this problem on the cathode side, the supply manifold pressure and a nominal supply manifold/cathode pressure drop are used in place of the cathode pressure. The anode supply manifold, on the other hand, is typically small and its volume is lumped in the present model with the anode volume. The anode pressure, P_{An} , can then be considered as being practically equal to the pressure in the anode supply manifold. The fuel inlet flowrate can, hence, be defined as $W_{An, in} = K_1(K_2 p_{SM} - p_{An})$, where K_1 is the fuel flowrate proportional gain, while $K_2 = p_{Ca}/p_{SM}$ is the pressure drop between the supply manifold and the cathode. It should be noted that to implement the proportional feedback controller for the fuel flowrate, the anode pressure, p_{An} , must be measured. Nevertheless, the anode pressure is not added to the list of measured variables in equation (17), since this equation is used to define the air flowrate control problem.

3 COMPUTATIONAL METHOD

Nine first-order non-linear ordinary differential equations, equations (1) to (9), are solved using the commercial mathematical and visualization package, MATLAB [10]. ODE23s MATLAB-solver based on a combination of second- and third-order Runge–Kutta methods is used. This solver is suitable for solving stiff differential equations whose response changes rapidly over a timescale that is short compared to the timescale over which the solution is sought.

The design of the feedback controller, discussed in section 4.2, is carried out using the Control System Toolbox of the MATLAB program [10]. The Control System Toolbox is a collection of algorithms that implements common control system design, analysis, and modeling techniques.

4 RESULTS AND DISCUSSION

4.1 Model linearization

In this section, a feedback controller is designed that cancels efficiently the disturbance of λ_{O_2} during the transient following abrupt changes in I_{st} . To develop such a controller, the plant is first linearized around a nominal operating point associated with the maximal net power, $P_{net}^{max} = 39.825$ kW, and the optimal oxygen excess ratio, $\lambda_{O_2}^{opt} = 2.33$, the stack current, $w^0 = I_{st} = 190$ A, and the compressor-motor voltage, $u^0 = v_{CM}^{opt} = 187.5$ V, where a superscript zero is used to denote the nominal value of a quantity. The linearization of the non-linear model defined by equations (1) to (9) is done by imposing a small perturbation around the nominal point to one of the states, the disturbance, or the control variable at a time, and quantifying the system response using a finite difference method. The resulting linearized model can be expressed as

$$\begin{aligned}\delta\dot{x} &= \mathbf{A}\delta x + \mathbf{B}_u\delta u + \mathbf{B}_w\delta w \\ \delta z &= \mathbf{C}_z\delta x + \mathbf{D}_{zu}\delta u + \mathbf{D}_{zw}\delta w \\ \delta y &= \mathbf{C}_y\delta x + \mathbf{D}_{yu}\delta u + \mathbf{D}_{yw}\delta w\end{aligned}\quad (18)$$

where δ is used to denote the variation of a quantity from its nominal value.

Linearized system matrices \mathbf{A} , \mathbf{B}_u , \mathbf{B}_w , \mathbf{C}_z , \mathbf{D}_{zu} , \mathbf{D}_{zw} , \mathbf{C}_y , \mathbf{D}_{yu} , and \mathbf{D}_{yw} are listed in Appendix A. It should be noted that while deriving matrices \mathbf{B}_w , \mathbf{D}_{zu} , and \mathbf{D}_{zw} of the linearized system, the effect of the current density on the optimal steady state value of the compressor-motor voltage (included as a static feedforward controller) has been taken into account. An analysis of the non-linear model carried out in our previous work [9] revealed that $m_{w, Ca}$ is associated with fully humidified air. Since the effect of vapour condensation in the cathode on the cathode permeability and, hence, on the FC voltage (the phenomenon generally referred to as cathode flooding) is not considered, the mass of water in the cathode is not an observable state and, therefore, is not considered in design of the feedback controller. In other words, the linearized system has eight states, one less than the original (non-linear) system. The eight linearized system states and their order are consistent with those listed in equation (17).

Application of a feedforward control strategy to regulate the transient behaviour of a PEMFC system, utilized in our previous work [9], revealed the presence of steady state errors in the performance variables ($z_1 = P_{net} - P_{net}^{max}$, $z_2 = \lambda_{O_2} - \lambda_{O_2}^{opt}$). To eliminate such steady state errors, an additional integral state variable is introduced. Since the performance variable of interest,

λ_{O_2} , cannot be directly measured, the integral variable had to be derived using the measured variables listed in equation (17). Since the compressor flowrate, $y_1 = W_{CP}$, can be readily measured and, as found in our recent work and reproduced in Fig. 2(b), its target value, W_{CP}^{opt} can be represented by the following second-order polynomial in terms of the stack current, I_{st} : $W_{CP} = -4.01 \times 10^{-7} I_{st}^2 + 4.03 \times 10^{-4} I_{st} - 0.0015$; this measured variable is used to define the integral state variable, q , as

$$\dot{q} = \delta W_{CP} - \delta W_{CP}^{opt} \quad (19)$$

Based on the linearized system states defined so far, the feedback control of the control variable, $u = v_{CM}$, can be designed as $\delta u = -K_p(\delta x - \delta x_d) - K_I q$, where K_p and K_I are the feedback proportional and the integral control gains respectively, and where $\delta x_d = x_d - x^0$ are deviations of the desired (steady state) states values, x_d , corresponding to the imposed stack current disturbance, δw , from the nominal states values, x^0 . The desired states, x_d , are obtained by solving states equations (1) to (9) or the first equation in equation (18), under the steady state condition.

The proportional and the integral gains are computed using the linear quadratic regulator (LQR) method to minimize the system response $\delta z_2 = \delta \lambda_{O_2} - \delta \lambda_{O_2}^{opt}$, and the steady state error without using excessive control. As shown in Fig. 2(c), the optimal value of the oxygen excess ratio, $\lambda_{O_2}^{opt}$, can be expressed as the following second-order polynomial in terms of the current $\lambda_{O_2}^{opt} = -2.7633 \times 10^{-6} I_{st}^2 - 15.931 \times 10^{-4} I_{st} + 2.7331$. The appropriate cost function is then defined as

$$J = \int_0^{\infty} \delta z_2^T Q_z \delta z_2 + q^T Q_1 q + \delta u^T R \delta u dt \quad (20)$$

Next, since δz_2 is affected by the disturbance δw , a new performance variable $\delta z' = C_{z_2} \delta x$ (C_{z_2} is the second row of matrix C_z) is introduced and the cost function is redefined as

$$J = \int_0^{\infty} \delta x^T C_{z_2}^T Q_z C_{z_2} \delta x + q^T Q_1 q + \delta u^T R \delta u dt \quad (21)$$

where $Q_z = 10^3$, $Q_1 = 10^{-3}$, and $R = 0.03$ are the appropriate weighting functions.

After adding q to the states vector δx and defining $q = [Q_x \quad Q_1]^T$, where $Q_x = C_{z_2}^T Q_z C_{z_2}$, the optimal gain is computed as $K = [K_p \quad K_I]^T = R^{-1} B^T \bar{P}$, where \bar{P} is the solution to the algebraic Riccati equation

$$\bar{P}A + A^T \bar{P} + Q - \bar{P}BR^{-1}B^T \bar{P} = 0 \quad (22)$$

This procedure yielded the following values of the proportional and integral gains

$$K_p = \begin{bmatrix} -23.612 & -3.2 \times 10^{-13} & -47.405 & 7.1853 \\ 412.7 & 2.6014 & -1.5 \times 10^{-13} & -168.57 \end{bmatrix}$$

$$K_I = -0.18257$$

(23)

4.2 Observer design

Since not all the states of the system can be directly measured, the measured variables, $y = [W_{CP}, p_{SM}, v_{st}]$ have to be used to obtain state estimates, $\delta \hat{x}$. Towards that end, a Kalman-filter-based state observer is constructed and used in the feedback control of the compressor motor voltage. The Kalman filter is a computational algorithm for determination of the optimum states estimates in a linearized system that utilizes initial conditions, a time sequence of system measurements, and statistical errors of the model and the measurements. Since the three measured variables: the compressor air flowrate, $y_1 = W_{CP}$; the supply manifold pressure, $y_2 = p_{SM}$; and the FC stack voltage, $y_3 = v_{st}$, provide a sufficient insight into the performance of a PEMFC system and are relatively easy to measure, they are selected for the construction of the state observer.

When using an observer to control the system, the issues of observability (the ability of measured variables to observe changes in all states) must be resolved. This is done with the help of the results given in Table 3 in which the system eigenvalues, ϵ_i , the corresponding eigenvectors and the rank and condition number of the matrix $E_{Obs} = [\epsilon_i I - A \quad C_y]^T$ are given, where I is an (8×8) identity matrix. The results displayed in this table show that the rank of matrix E_{Obs} is 8. This indicates that the system is observable with respect to all eight eigenvalues. However, the condition number of the matrix, E_{Obs} associated with the least negative eigenvalue ($\epsilon_8 = -1.1525$) is quite large, indicating a weak observability of this eigenvalue. This is of major concern since it can result in degradation of the observer performance, primarily giving rise to large observer gains and to large overshoots in the observer error. To prevent this from happening, a reduced-order output estimator (close-loop observer) is implemented for the observable part of the system.

The first step towards developing such a reduced-order observer is to transform the linearized system to the modal canonical form as: $\delta x_c = T \delta x$, where T is the canonical transformation matrix. The resulting system matrices in the canonical coordinate system are: $A_c = T A T^{-1}$, $B_c = T [B_w \quad B_u]$ and $C_c = C_y T^{-1}$, where A_c is a diagonal matrix with its diagonal elements equal to the system eigenvalues (given in Table 3). These matrices

Table 3 Eigenvalues, eigenvectors, and observability

Eigenvalues								
ϵ	-220.28	-90.191	-46.551	-40.454	-14.914	-3.0523	-1.9536	-1.1525
Eigenvectors								
$\times 1$	1.91E-16	-0.17417	-0.08597	1.07E-16	0.0572	0.03	-0.90254	-0.12206
$\times 2$	-0.2928	0.01242	-0.03003	-0.14855	0.00355	-0.01362	-0.00715	-0.00578
$\times 3$	-9.12E-17	-0.74689	-0.08821	-4.51E-17	0.16936	-0.41992	0.15873	-0.11454
$\times 4$	-2.94E-16	-0.12388	-0.3857	-5.72E-16	0.97716	-0.83021	-0.39835	-0.3031
$\times 5$	1.88E-17	0.04815	0.06507	9.22E-17	0.00908	-0.04192	-0.02232	-0.01821
$\times 6$	-5.39E-17	0.61447	0.82538	8.73E-16	0.11172	-0.36061	-0.0224	-0.93782
$\times 7$	-0.95617	0.08276	0.36736	0.9889	-0.00389	0.0044	0.00192	0.00133
$\times 8$	8.52E-18	0.09788	-0.12137	-1.50E-16	0.02466	-0.03892	-0.0221	-0.01546
Observability								
rank ($\epsilon I-A; C_y$)	8	8	8	8	8	8	8	8
cond ($\epsilon I-A; C_y$)	220.43	148.62	228.71	504.38	322.26	898.35	1374.8	2286.2

are next partitioned as

$$A_c = \begin{bmatrix} A_{cu} & 0 \\ 0 & A_{cd} \end{bmatrix}, \quad B_c = \begin{bmatrix} B_{cu} \\ B_{cd} \end{bmatrix}$$

and

$$C_c = [C_{cu} \quad C_{cd}]$$

in order to separate the observable and the weakly observable parts of the system.

Next, matrices A_{cu} , B_{cu} and C_{cu} are used to compute the reduced-order observer gains, L_u , using the linear quadratic Gaussian method as

$$L_u = S C_{cu}^T W_y^{-1} \tag{24}$$

where S is the solution of the following equation

$$0 = S A_{cu}^T + A_{cu} S + V_x + S C_{cu}^T W_y^{-1} C_{cu} S \tag{25}$$

and W_y and V_x are positive definite weighting matrices representing the intensities of measurement noise and process disturbance respectively. They are assigned the following values consistent with the stochastic Kalman estimator design [11]

$$V_x = \text{diag}[0.01 \quad 10 \quad 10 \quad 0.01 \quad 10 \quad 10 \quad 10] + \alpha B_{cu} B_{cu}^T \tag{26}$$

$$W_y = 1 \times 10^{-6} \text{diag}[10 \quad 100 \quad 1] \tag{27}$$

and $\alpha = 30$.

The reduced-order observer gain, L_u , is then transformed to the original coordinate system as $L = T^{-1}[L_u \quad 0]^T$

to yield

$$L = \begin{bmatrix} -27.748 & 1.5294 & 2931.4 \\ -3.6069 & 2.5225 & 26.477 \\ -23.346 & 83.781 & -349.02 \\ 6415.1 & 447.48 & 211.72 \\ -33.486 & 16.822 & 40.620 \\ -716.97 & 148.83 & -234.87 \\ -190.78 & 19.455 & -69.945 \\ -1.0835 & 5.8859 & 66.991 \end{bmatrix} \tag{28}$$

In the presence of an observer, the linearized system can then be represented as:

$$\begin{aligned} \delta \dot{x} &= A \delta x + B_u \delta u + B_w \delta w + L(\delta y - \delta \hat{y}) \\ \delta z &= C_z \delta x + D_{zu} \delta u + D_{zw} \delta w \\ \delta \hat{y} &= C_y \delta x + D_{yu} \delta u + D_{yw} \delta w \end{aligned} \tag{29}$$

where $\hat{\cdot}$ is used to denote observer estimated quantities and

$$u = -K_p(\delta \hat{x} - \delta x_d) - K_I q \tag{30}$$

4.3 Simulations

In this section, the results of simulations of the transient response of the stack current system are presented and discussed. A schematic of the observer-based feedback controller used is shown in Fig. 3.

A time evolution of the stack current consisting of a number of steps that acts as an input disturbance to the system is shown in Fig. 4(a). The corresponding

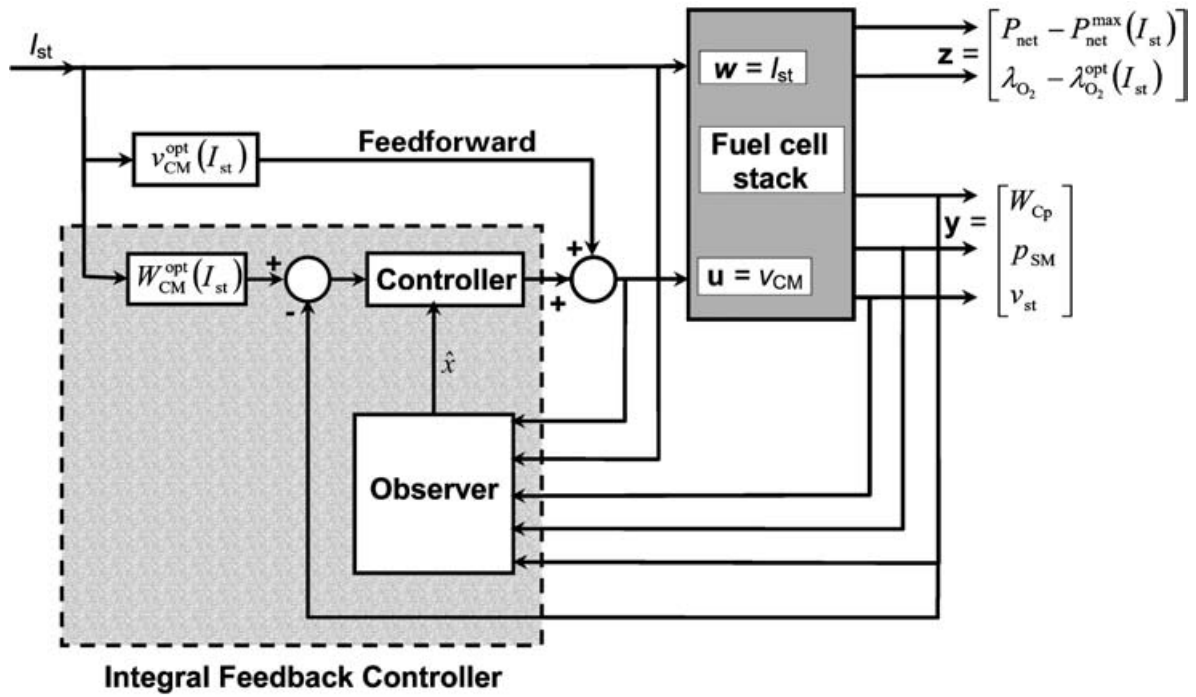


Fig. 3 Observer-based feedback controller for a PEMFC system

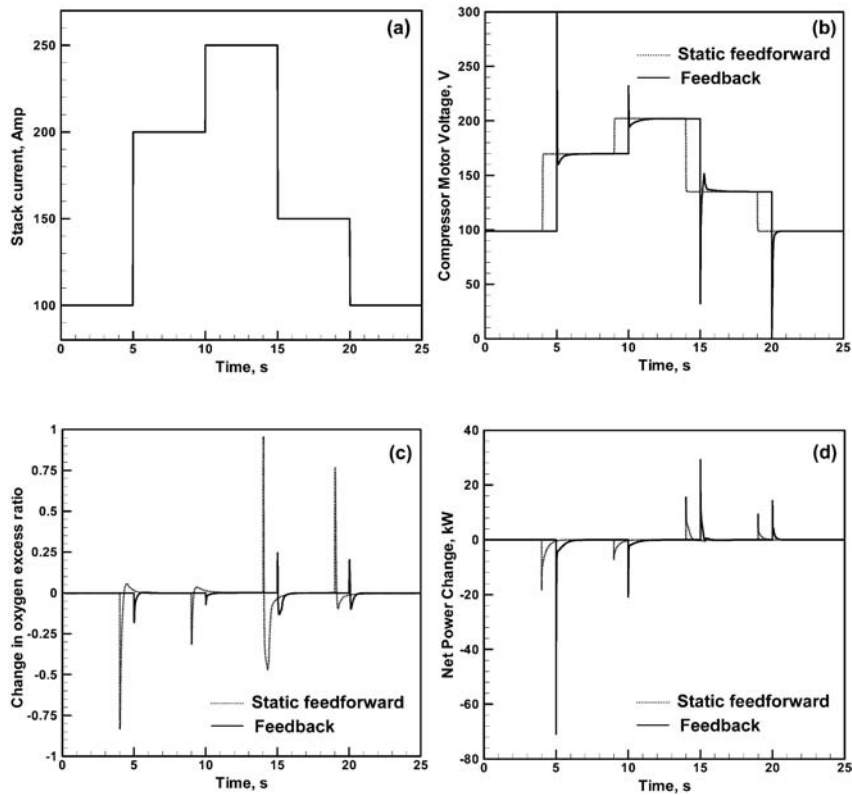


Fig. 4 (a) Step-like temporal variation of the (input) stack current, and (b) the corresponding compressor-motor voltage; (c) change in oxygen excess ratio; and (d) change in net power for static feedforward and observer-based, feedback-controlled levels

variation in the compressor-motor voltage, the controlled input, is shown (as a solid line) in Fig. 4(b). The static feedforward component of the v_{CM} is also shown in Fig. 4(b), but as a dotted line. The time evolution of the two performance variables, $z_1 = P_{net} - P_{net}^{max}$ and $z_2 = \lambda_{O_2} - \lambda_{O_2}^{opt}$ for both the static feedforward and the feedback-controlled PEMFC systems are shown in Figs 4(c) and (d) respectively. To improve clarity, the dotted lines in Figs 4(b) to (d), pertaining to the results for the static feedforward controller, are shifted to the left along the time axis by 1 s.

The results displayed in Fig. 4(b) show that the v_{CM} versus I_{st} relationship for the static feedforward controller consists of a number of steps in accordance with the optimal value of the compressor-motor voltage, v_{CM}^{opt} , which at a given level of the stack current ensured an optimal level of the oxygen excess ratio, $\lambda_{O_2}^{opt}$. For the feedback controller, on the other hand, the compressor-motor voltage has a transient behaviour that efficiently rejects the λ_{O_2} disturbance following an abrupt change in the stack current. Nevertheless, after the transient, v_{CM} , attains its optimal value consistent with the v_{CM}^{opt} versus I_{st} relationship.

The results displayed in Fig. 4(c) show that both the static feedforward controller based on the v_{CM}^{opt} versus I_{st} relationship and the observer-based feedback controller perform quite well with respect to maintaining the oxygen excess ratio at the optimal value consistent with a given input level of the stack current. However, the feedforward controller suffers from a number of deficiencies, such as:

- its rise and its settling times are relatively long;
- transient behaviour involves an overshoot;
- it is sensitive to modelling errors, ageing of the fuel stack components and variations in ambient conditions; and
- because there is no feedback, the sensitivity of the system being controlled to unknown disturbances is equal to unity at all frequencies.

Magnitude of the sensitivity function at different frequencies for the observer-based feedback controller is shown in Fig. 5. It is seen that except at very high frequencies, system sensitivity to input uncertainties is substantially smaller than unity. Also, for a single input–single output system, the inverse of the sensitivity magnitude is a measure of the distance from system instability. Thus, small values of the sensitivity for the feedback controller indicate a large robustness of the system (i.e. relatively large variations in the system parameters are required to cause instability). Taking all this into account, the performance of the feedback controller can be considered as superior relative to that of the static feedforward controller with respect to maintaining the optimal level of the oxygen excess ratio.

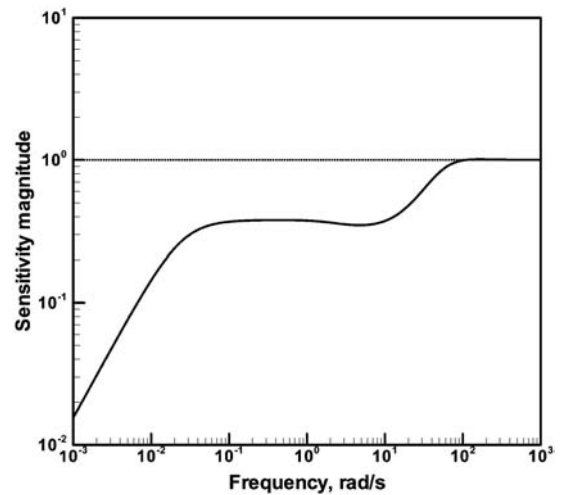


Fig. 5 Frequency dependence of the input-sensitivity magnitude for the PEMFC system with an observer-based feedback controller

The results displayed in Fig. 4(d) show that the improvements in the performance of the feedback controller with respect to maintaining the optimal level of the oxygen excess ratio are achieved at the expense of transient behaviour of the system net power. In general, significantly larger perturbations in the system net power and longer settling times are found in the case of the feedback controller.

The transient dynamic response of the compressor (represented by the appropriate air flowrate versus compression ratio trajectories on the compressor map) and the associate dynamic electrical response of the FC (represented by the appropriate voltage versus current-density trajectories on the polarization plot) for the FC system regulated by the feedback are shown in Figs 6(a) and (b) respectively. The results displayed in Fig. 6(a) can be used to identify stack-current changes, which may produce a surge or a stall of the compressor, while the results displayed in Fig. 5(b) can be used to determine the effective electrical resistance of the controlled FC stack.

In summary, step changes in the stack current require rapid adjustments in the air flow, as well as of the fuel flow. In a case when the stack current undergoes a step increase, a rapid increase in the air flow is required to prevent oxygen depletion in the cathode. If the air compressor motor is powered by the FC stack itself, this may require a large amount of power, which causes the net power to decrease. Thus, the transfer function from the control variable to the net power is a non-minimum phase.

The control problem analyzed in this paper is a single-input–single-output problem in which a single-input variable, v_{CM} , is used to control a single-output variable, λ_{O_2} . In other words, when the stack current, I_{st} ,

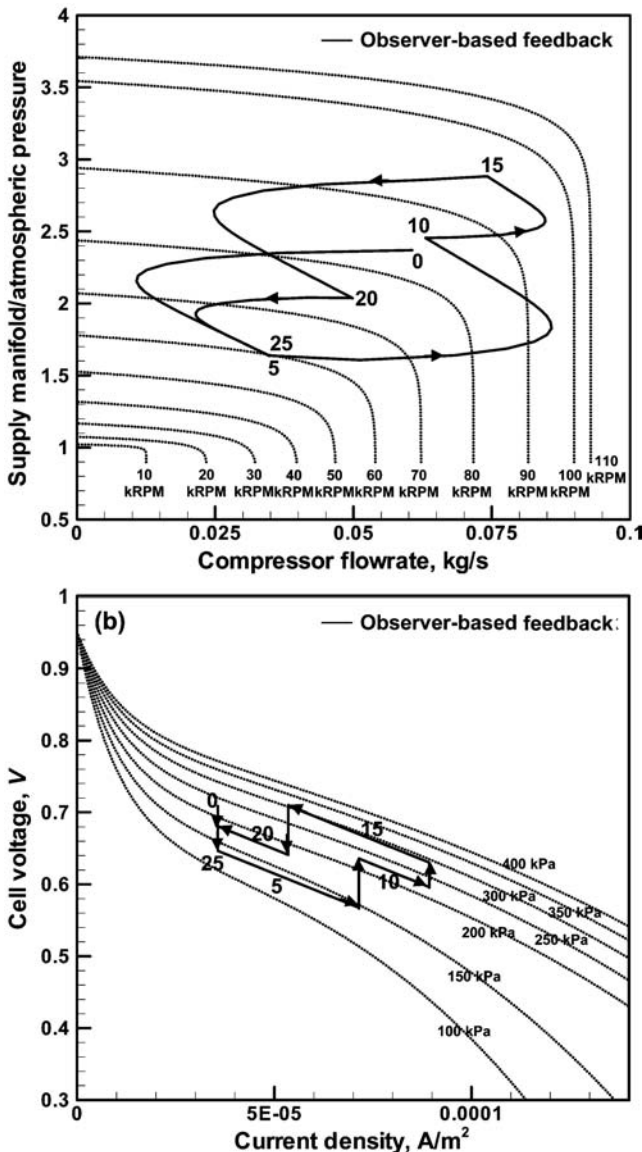


Fig. 6 Temporal responses of: (a) the compressor and (b) the FC corresponding to the changes in the stack current displayed in Fig. 4(a) under the observer-based feedback control of the compressor-motor voltage. The numbers associated with arrowed lines refer to the time in seconds

changes, the compressor-motor voltage, v_{CM} , is promptly adjusted to attain the new optimal level of the oxygen excess ratio, $\lambda_{O_2}^{opt}$. A comparison of the results for the static feedforward and for the observer-based feedback controller displayed in Figs 4(c) and (d) shows that the use of the feedback controller reduces the time needed for λ_{O_2} to attain its new optimal value following a stack current step change. However, this is accomplished at the expense of the time required for the net power to achieve its respective new maximum value, P_{net}^{max} . The trade-off between the P_{net}^{max} and the $\lambda_{O_2}^{opt}$ transient responses cannot be eliminated because there is only

one control variable, v_{CM} . Thus, if v_{CM} is used to control λ_{O_2} , a separate power source (e.g. an electric battery) is required to regulate the transient response of P_{net} .

5 CONCLUSIONS

Based on the results obtained in this paper, the following main conclusions can be drawn:

1. The dynamic model for PEMFC systems developed by Pukrushpan *et al.* [7–8], while not validated experimentally, appears to capture the basic transient behaviour of PEMFC systems, including air-flow characteristics and dynamics of the air compressor motor and the supply manifold filling.
2. A feedforward or a feedback control scheme can be readily implemented to prevent large excursions in the oxygen excess ratio during abrupt changes in the stack current. While a static feedforward controller, which can be easily constructed, is found to perform quite well, due to its high sensitivity to unpredicted external disturbances and errors in model parameters due to equipment, the use of a feedback controller is preferred.
3. The use of an observer-based integral feedback controller reduces the rise and the settling time for the oxygen excess ratio during the transient following abrupt changes in the step current relative to their counterparts in the case of a feedforward controller. However, this is accompanied by a compromise in the transient behaviour of the net power of the PEMFC system. This finding reveals the need for a separate FC power management strategy.

REFERENCES

- 1 Yang, W.-C., Bates, B., Fletcher, N. and Pow, R. Control challenges and methodologies in fuel cell vehicle development, SAE Paper, No. 98C054.
- 2 Grujicic, M. and Chittajallu, K. M. Design and optimization of polymer electrolyte membrane (PEM) fuel cells, *Appl. Surface Sci.*, 2004, **227**, 56–72.
- 3 Grujicic, M. and Chittajallu, K. M. Geometrical optimization of the cathode in polymer electrolyte membrane (PEM) fuel cells, *Chem. Eng. Sci.*, 2004, accepted for publication.
- 4 Grujicic, M. and Chittajallu, K. M. Cathode and interdigitated air distributor optimizations in polymer electrolyte membrane (PEM) fuel cells, *Mat. Sci. Eng., B*, 2004, **108**, 241–252.
- 5 Hauer, K. H., Friedmann, D. J., Moore, R. M., Ramaswamy, S., Eggert, A. and Badrinarayana, P. Dynamic response of an indirect-methanol fuel cell vehicle, SAE Paper, 2000, No. 2000-01-370.
- 6 Pischinger, S., Schonfelder, C., Bornscheuer, W., Kindl, H. and Wiartalla, A. Integrated air supply and humidification concepts for fuel cell systems, SAE Paper, 2001, No. 2001-01-0233.

- 7 Pukrushpan, J. T., Peng, H. and Stefanopoulou, A. G. Simulation and analysis of transient fuel cell system performance based on a dynamic reactant flow model. ASME International Mechanical Engineering Congress and Exposition, New Orleans, LA, USA, November 17–22, 2002.
- 8 Pukrushpan, J. T., Stefanopoulou, A. G. and Peng, H. Modeling and control for PEM fuel cell stack system. Proceedings of the American Control Conference, Anchorage, AK, USA, 2002, pp. 3117–3122.

- 9 Grujicic, M., Chittajallu, K. M., Law, E. H. and Pukrushpan, J. T. Transient behavior and control of polymer electrolyte membrane (PEM) fuel cell systems, *Appl. Surface Sci.*, 2004, accepted for publication.
- 10 MATLAB. *The Language of Technical Computing*, 6th edn (The MathWorks Inc., 24 Prime Park Way, Natick, MA, USA), 01760-1500, 2000.
- 11 Anderson, B. D. O. and Moore, J. B. *Optimal Control: Linear Quadratic Methods*, 1989 (Prentice-Hall, NJ, USA).

APPENDIX A: LINEARIZED SYSTEM MATRICES

The system matrices obtained by linearizing the non-linear model of the PEMFC around a nominal point corresponding to $P_{\text{net}}^{\text{max}} = 39.825$ kW, $I_{\text{st}} = 190$ A, $v_{\text{CM}}^{\text{opt}} = 187.5$ V, and $\lambda_{\text{O}_2}^{\text{opt}} = 2.33$ are given below

$$\mathbf{A} = \begin{bmatrix} -6.5421 & 0 & -10.8897 & 0 & 83.8255 & 0 & 0 & 24.52081 \\ 0 & -161.099 & 0 & 0 & 49.4407 & 0 & -18.1228 & 0 \\ -18.68 & 0 & -46.8923 & 0 & 275.926 & 0 & 0 & 161.4285 \\ 0 & 0 & 0 & -13.0714 & 198.433 & 0 & 0 & 0 \\ 1.2956 & 0 & 2.96019 & 0.36814 & -39.968 & 0.104351 & 0 & 0 \\ 16.641 & 0 & 38.0211 & 4.72839 & -488.88 & 0 & 0 & 0 \\ 0 & -393.984 & 0 & 0 & 117.852 & 0 & -99.637 & 0 \\ 2.022 & 0 & 4.61989 & 0 & 0 & 0 & 0 & -51.3409 \end{bmatrix}$$

$$\mathbf{B}_u = \begin{bmatrix} 0 \\ 0 \\ 0 \\ 2.7569 \\ 0 \\ 0 \\ 0 \\ 0 \end{bmatrix} \quad \mathbf{B}_w = \begin{bmatrix} -0.03159 \\ -0.00395 \\ 0 \\ 2.681436 \\ 0 \\ 0 \\ -0.09025 \\ 0 \end{bmatrix} \quad \mathbf{D}_{zu} = \begin{bmatrix} -0.16898 \\ 0 \end{bmatrix} \quad \mathbf{D}_{zw} = \begin{bmatrix} -0.10412 \\ -0.01042 \end{bmatrix}$$

$$\mathbf{D}_{yu} = \begin{bmatrix} 0 \\ 0 \\ 0 \end{bmatrix} \quad \mathbf{D}_{yw} = \begin{bmatrix} 0 \\ 0 \\ -0.32468 \end{bmatrix}$$

$$\mathbf{C}_z = \begin{bmatrix} 2.66013 & 2.03688 & -0.10896 & 0.1244 & 0 & 0 & 0 & 0 \\ -0.63705 & 0 & -1.45555 & 0 & 13.8927 & 0 & 0 & 0 \end{bmatrix}$$

$$\mathbf{C}_y = \begin{bmatrix} 0 & 0 & 0 & 4.72839 & -125.977 & 0 & 0 & 0 \\ 0 & 0 & 0 & 0 & 1 & 0 & 0 & 0 \\ 13.9274 & 10.6643 & -0.57047 & 0 & 0 & 0 & 0 & 0 \end{bmatrix}$$